Suppression of stimulated Raman scattering by an electromagnetically-induced-transparency–like scheme and its application for super-resolution microscopy

Li Gong* and Haifeng Wang
Department of Physics, National University of Singapore, Singapore, 117542
(Received 4 June 2015; published 17 August 2015)

We theoretically investigate a scheme in which stimulated Raman scattering (SRS) can be suppressed by coherently controlling the coupling between molecular states. In conventional SRS, two laser beams at different frequencies interact resonantly with molecular vibration to induce a gain and a loss for the two beams, respectively. In our scheme, a third beam is introduced to couple the vibrational state to another coupling state. As a result, SRS is suppressed in a way analogous to electromagnetically induced transparency. We calculated the SRS signal analytically by the density matrix approach, and investigated the feasibility of this scheme for real molecular imaging. In SRS microscopy, a donut-shaped coupling laser can be used to suppress the SRS signal from the rim part of the focal spot, leading to super-resolution. Based on our numerical studies, the lateral resolution starts to be enhanced when the coupling laser intensity exceeds 0.1 TW/cm^2 at picosecond pulse duration.

DOI: 10.1103/PhysRevA.92.023828 PACS number(s): 42.65.Dr

I. INTRODUCTION

Coherent Raman imaging methods such as coherent anti-Stokes Raman scattering (CARS) microscopy [1,2] and stimulated Raman scattering (SRS) microscopy [3,4] are advanced nonlinear optical imaging methods. In these methods, two laser beams at different frequencies called the pump (ω_p) and Stokes ($\omega_S < \omega_p$) are focused into a sample. Raman resonance happens when $\omega_p - \omega_S$ matches the frequency of a molecular vibrational level. CARS detects the output at a new frequency $2\omega_p - \omega_S$ which is enhanced by Raman resonance, and SRS detects the loss of the pump beam or the gain of the Stokes beam caused by the resonant excitation of molecules to the vibrational level. Both methods are very attractive for biomedical applications due to their label-free nature, chemical selectivity, and high sensitivity. However, their spatial resolution is conventionally determined by the size of the diffraction-limited focal spots. The lateral resolution is usually limited to $\lambda/3$–$\lambda/2$.

In fluorescent microscopy, the diffraction limit has been broken by several elegant methods successfully, such as stimulated-emission-depletion (STED) microscopy [5], stochastic-optical-reconstruction microscopy (STORM) [6], and structured-illumination microscopy (SIM) [7]. In CARS microscopy, achieving super-resolution in the far field is also of interest and some schemes have been proposed in the last few years [8–15]. Many of them resemble STED microscopy [8,11–14], in which a donut-shaped beam is used to diminish the signal from the rim part of the focal spot. Thus the size of the effective excitation volume is reduced.

Compared with CARS, SRS microscopy has the advantage that it is intrinsically free of nonresonant background [3]. Some of the super-resolution techniques for CARS microscopy mentioned above may still be valid for SRS microscopy, such as reported in Ref. [8]. We also presented a STED-like super-resolution SRS microscopy scheme in our previous study [16]. However, these methods mostly rely on the saturated excitation of an electronic state or vibrational state, which may increase the tendency of photodamage in real applications.

In this study, we propose a scheme to suppress the SRS signal by the destructive interference between two quantum absorption pathways which is analogous to electromagnetic induced transparency (EIT) [17–19]. Another excitation state and a coupling laser have to be introduced in this scheme. But just like in EIT, most of the molecules will stay at the ground state, and so this method is better at avoiding photodamage. In this paper, we will introduce the theoretical study on this scheme, and numerically investigate the resolution enhancement if it is applied in STED-like super-resolution SRS microscopy.

II. THEORETICAL FRAMEWORK

Figure 1(a) illustrates the energy diagram of SRS, in which the sample is illuminated by the pump and Stokes lasers at frequencies ω_p and ω_S, respectively. The sample has a ground state $|g\rangle$ and a vibrational state $|v\rangle$ and a lot of intermediate states $|i\rangle$ which can couple with both $|g\rangle$ and $|v\rangle$ by dipole transition. When the frequency difference $\omega_p - \omega_S$ matches the frequency of the molecular vibrational frequency ω_{vg}, a net transition from $|g\rangle$ to $|v\rangle$ will occur due to Raman resonance. Because of this transition, the pump beam experiences a loss in the medium and the Stokes beam experiences a gain. They are called stimulated Raman loss (SRL) and stimulated Raman gain (SRG), respectively, which are the two aspects of SRS. Either SRL or SRG can be detected as the signal in SRS microscopy.

Figure 1(b) shows an energy diagram of EIT in a ladder scheme [19]. A probe laser at frequency ω_{pr} couples states $|1\rangle$ and $|2\rangle$ and a strong coupling laser at frequency ω_c couples states $|2\rangle$ and $|3\rangle$. In an interaction picture, under the rotating wave approximation (RWA), the first-order perturbation of the Schrödinger's equation reads [20]

$$\dot{C}_2^{(1)} - i(\delta + i\gamma_{21})C_2^{(1)} = i\Omega_{pr} + iC_3^{(1)}\Omega_c, \quad (1a)$$

$$\dot{C}_3^{(1)} - i(\delta - \Delta + i\gamma_{31})C_3^{(1)} = iC_2^{(1)}\Omega_c^*, \quad (1b)$$

where C_2 and C_3 are the probability amplitude of state $|2\rangle$ and $|3\rangle$; γ_{ab} is the decoherent rate between state $|a\rangle$ and $|b\rangle$; Ω_{pr} and Ω_c are the Rabi frequencies of probe and coupling lasers; $\delta = \omega_{pr} - \omega_{21}$ and $\Delta = \omega_c - \omega_{32}$ are the detuning of the probe and coupling lasers, respectively. The steady-state

*Corresponding author: phygoli@nus.edu.sg

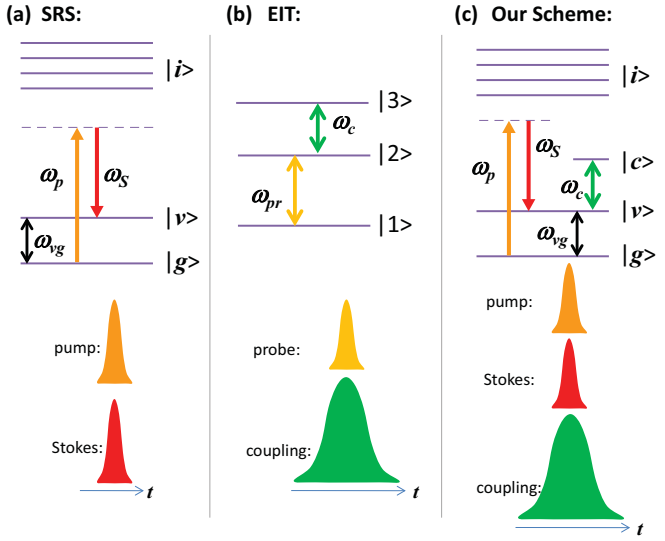

FIG. 1. (Color online) Energy level diagrams. (a) SRS: a pump beam and a Stokes beam are used to match the transition from ground state $|g\rangle$ to a vibrational state $|v\rangle$ via many intermediate states $|i\rangle$. (b) EIT in a ladder scheme: The probe laser couples state $|1\rangle$ and $|2\rangle$, while the coupling laser couples state $|2\rangle$ and $|3\rangle$. The coupling pulse is normally required to be stronger and wider than the probe pulse to satisfy the adiabatic approximation. (c) Our scheme: replace the $|1\rangle$ to $|2\rangle$ one-photon transition in EIT with SRS from the ground state $|g\rangle$ to the vibrational state $|v\rangle$.

solution of Eq. (1) shows that when Ω_c is large enough, C_2 will always be close to 0. It means that the absorption of the probe laser can be suppressed when the coupling laser is strong enough. Intuitively, it is because there are two possible quantum pathways that lead to the same final state: $|1\rangle \rightarrow |2\rangle$ and $|1\rangle \rightarrow |2\rangle \rightarrow |3\rangle \rightarrow |2\rangle$, and the probability amplitudes of these two pathways destructively interfere. As a result, the total transition from $|1\rangle$ to $|2\rangle$ is suppressed and so is the absorption of probe photons.

If the sample is illuminated by pulsed lasers, in order to keep the steady-state solution of Eq. (1) valid all the time, the change of Ω_{pr}/Ω_c should be slow enough to satisfy adiabatic approximation; i.e., we need a stronger and wider coupling pulse than the probe pulse [19], as illustrated in Fig. 1(b).

In our scheme, the one-photon transition $|1\rangle$ to $|2\rangle$ in EIT is replaced by multiphoton SRS from the ground state $|g\rangle$ to the vibrational state $|v\rangle$, as shown in Fig. 1(c). A coupling laser at frequency ω_c then couples the vibrational state $|v\rangle$ and a coupling state $|c\rangle$ by dipole transition. Similar to EIT, in this case there are two quantum pathways to the same final state: $|g\rangle \rightarrow |v\rangle$ and $|g\rangle \rightarrow |v\rangle \rightarrow |c\rangle \rightarrow |v\rangle$. Therefore it can be expected that if the excitation laser fields are designed properly, the two pathways will destructively interfere, resulting in the suppression of SRS.

Mathematically, with CW excitations we can easily obtain similar equations like Eq. (1) to describe our scheme, just by replacing Ω_{pr} with the two-photon Rabi frequency of SRS transition. Then we can derive a similar steady-state solution which will show the suppression of SRS. However, normally tightly focused femtosecond or picosecond excitations are required in SRS microscopy since SRS is a third-order nonlinear process [3]. In this regard, it is necessary to study the evolution of our system with pulsed excitations. However, we have to study the case in which the pulse duration is comparable to the relaxation time. A unique feature in our case is that the typical relaxation time of the vibrational state γ_{gv} is several hundred femtoseconds [21], at the same order of magnitude as the excitation pulse duration for SRS microscopy. This is different from most studies on EIT with pulsed excitations [22–27], where the pulse durations were either much longer or much shorter than the relaxation times between states.

Our mathematical model is as follows. For Gaussian pulses without chirp, the electric field in each pulse can be expressed as

$$\begin{aligned}\mathbf{E}_\alpha &= E_\alpha(t)\frac{e^{-i\omega_\alpha t}\mathbf{e}_\alpha + \text{c.c.}}{2} \\ &= A_\alpha \exp\left[-2\ln 2\left(\frac{t}{\tau_\alpha}\right)^2\right]\frac{e^{-i\omega_\alpha t}\mathbf{e}_\alpha + \text{c.c.}}{2},\end{aligned} \tag{2}$$

where the subscript α can be "p," "S," or "c," denoting pump, Stokes, or coupling light, respectively; A is the field amplitude, which is a real quantity; τ is the full width at half maximum (FWHM) in intensity; $\mathbf{e}$ is a complex unit vector which describes the phase and polarization of light.

Applying RWA, the Hamiltonian of our system under external classical light fields can be written as

$$\begin{aligned}\hat{H} = &-\frac{\hbar}{2}\sum_i[(\Omega_{S,gi}e^{-i\omega_S t} + \Omega_{p*,gi}e^{i\omega_p t})|g\rangle\langle i| \\ &+ (\Omega_{S*,vi}e^{i\omega_S t} + \Omega_{p,vi}e^{-i\omega_p t})|v\rangle\langle i| + \text{c.c.}] \\ &- \frac{\hbar}{2}(\Omega_{c,cv}e^{-i\omega_c t}|c\rangle\langle v| + \text{c.c.}) + \frac{\hbar}{2}\sum_{l=g,i,v,c}\omega_l|l\rangle\langle l|,\end{aligned} \tag{3}$$

where $\Omega_{\alpha,lm} = E_\alpha(t)\mathbf{e}_\alpha \times \boldsymbol{\mu}_{lm}$ and $\Omega_{\alpha^*,lm} = E_\alpha(t)\mathbf{e}_\alpha^* \cdot \boldsymbol{\mu}_{lm}$ are the time-dependent Rabi frequencies of transition $|l\rangle$ to $|m\rangle$ caused by pulse α. $\boldsymbol{\mu}_{lm}$ is the transition dipole vector.

Since the decoherence between states must be considered in SRS, we have to treat this problem by a density matrix approach, in which the status of the sample is described by a density matrix ρ_{lm}, where l, $m = g$, i, v, or c. The evolution of ρ is governed by a Liouville–von Neumann equation with phenomenological decoherence terms. Here we solve the equation in terms of perturbation expansion of $\mathbf{E}_p$ and $\mathbf{E}_S$. As in standard perturbation theory, $\mathbf{E}_p$ and $\mathbf{E}_S$ are replaced by $\lambda\mathbf{E}_p$ and $\lambda\mathbf{E}_S$, and ρ is expanded as a power series of λ: $\rho = \rho^{(0)} + \lambda\rho^{(1)} + \lambda^2\rho^{(2)}\cdots$ [20]. If we assume that the sample is at the ground state in the beginning, $\rho_{gg}^{(0)} = 1$ while other components of $\rho^{(0)}$ are zero. That is to say, most of the sample molecules stay at the ground state, as long as $\mathbf{E}_p$ and $\mathbf{E}_S$ can be regarded as perturbations.

The first-order perturbation of ρ can be solved in Fourier space:

$$\begin{aligned}\tilde{\rho}_{ig}^{(1)}(\omega) = \frac{1}{2}\Bigg\{&\frac{\tilde{\Omega}_{p,ig}(\omega+\omega_p)}{[\omega_{ig} - \omega_p + (\omega+\omega_p)] - i\gamma_{ig}} \\ &+ \frac{\tilde{\Omega}_{S*,ig}(\omega-\omega_S)}{[\omega_{ig} + \omega_S + (\omega-\omega_S)] - i\gamma_{ig}}\Bigg\},\end{aligned} \tag{4}$$

where "$\sim$" above a variable denotes its Fourier transformation.

The pulse duration of the pump laser (τ_p) used in SRS microscopy is from hundreds of femtoseconds to several

picoseconds. Therefore the bandwidth of $\tilde{\Omega}_{p,ig}$ is $1/\tau_p$ which is on the order of 10^0-10^1 THz. Thus in the first term on the right side of Eq. (4), when $|\omega+\omega_p|$ is larger than this range $\tilde{\Omega}_{p,ig}(\omega+\omega_p)$ decays to zero rapidly. The intermediate states $|i\rangle$ are electronic states for Raman scattering which usually lie in the UV-visible (vis) region, and so ω_{ig} is on the order of 10^3-10^4 THz. Since near-infrared (NIR) lasers are conventionally used as pump and Stokes light in SRS microscopy, ω_p is on the order of 10^3 THz. Thus $\omega+\omega_p$ can be ignored in the denominator of the first term, and so can $\omega-\omega_S$ in the denominator of the second term. After inverse Fourier transformation, we obtain

$$\rho_{ig}^{(1)}=\frac{1}{2}\left[\frac{\Omega_{p,ig}e^{-i\omega_p t}}{(\omega_{ig}-\omega_\alpha)-i\gamma_{ig}}+\frac{\Omega_{S*,ig}e^{i\omega_S t}}{(\omega_{ig}+\omega_\alpha)-i\gamma_{ig}}\right]. \quad (5)$$

When going to the second-order perturbation, there are two differential equations about $\rho_{vg}^{(2)}$ and $\rho_{cv}^{(2)}$. By introducing a rotating frame $\rho_{vg}^{(2)}=\rho_{vg}^{(2,I)}\exp[-i(\omega_p-\omega_S)t]$ and $\rho_{cg}^{(2)}=\rho_{cg}^{(2,I)}\exp[-i(\omega_p-\omega_S+\omega_c)t]$, we have

$$\dot{\rho}_{vg}^{(2,I)}=i(\Delta_1+i\gamma_{vg})\rho_{vg}^{(2)}+i\frac{\Omega_{\rm SRS}}{2}+i\frac{\Omega_{c*,vc}}{2}\rho_{cg}^{(2,I)}, \quad (6a)$$

$$\dot{\rho}_{cg}^{(2,I)}=i(\Delta_2+i\gamma_{cg})\rho_{cg}^{(2,I)}+i\frac{\Omega_{c,cv}}{2}\rho_{vg}^{(2,I)}, \quad (6b)$$

where the detuning $\Delta_1=\omega_p-\omega_S-\omega_{vg}$, $\Delta_2=\omega_p-\omega_S+\omega_c-\omega_{cg}$, and $\Omega_{\rm SRS}$ is an effective two-photon Rabi frequency. Based on Eq. (5), $\Omega_{\rm SRS}$ is expressed as

$$\Omega_{\rm SRS}=\frac{1}{2}\sum_{|i\rangle}\left[\frac{\Omega_{p,ig}\Omega_{S*,vi}}{\omega_{ig}-\omega_p-i\gamma_{ig}}+\frac{\Omega_{p,vi}\Omega_{S*,ig}}{\omega_{ig}+\omega_S-i\gamma_{ig}}\right]. \quad (7)$$

According to Eq. (7), this two-photon Rabi frequency will be nonzero when the pump and Stokes pulses are temporally overlapped. Thus we only consider the situation with $\tau_S=\tau_p=\tau$ in the following discussion.

Note that Eq. (6) has the same mathematical form as Eq. (1) for EIT. Hence, the Raman coherence ρ_{vg} can be suppressed in a similar way as C_2 is suppressed in EIT. In this work, we solved Eq. (6) for excitation pulses described in Eq. (2) analytically by a mean-field approach, i.e., replacing $\Omega_{c,cv}$ by an average Rabi frequency expressed in Eq. (8). As mentioned earlier, in EIT, the change of Ω_{pr}/Ω_c should be slow enough to satisfy adiabatic approximation. Otherwise, the probe light will experience a preparation loss [19]. Similarly, we need to make the change of $\Omega_{\rm SRS}/\Omega_{c,cv}$ slow enough in our scheme. That is to say, τ_c must be larger than $\tau_S=\tau_p=\tau$. In this case, the mean-field approach is a reasonable approximation. This approximation will be discussed more later in this section.

$$\bar{\Omega}_{c,cv}=\frac{\int_{-\infty}^{\infty}\Omega_{c,cv}\Omega_{\rm SRS}dt}{\int_{-\infty}^{\infty}\Omega_{\rm SRS}dt}. \quad (8)$$

Now Eq. (6) can be solved in Fourier space:

$$\tilde{\rho}_{vg}^{(2,I)}(\omega)=\frac{2(\omega-\Delta_2-i\gamma_{cg})\tilde{\Omega}_{\rm SRS}}{4(\omega-\Delta_1-i\gamma_{vg})(\omega-\Delta_2-i\gamma_{cg})-|\bar{\Omega}_{c,vc}|^2}, \quad (9a)$$

$$\tilde{\rho}_{cg}^{(2,I)}(\omega)=\frac{\bar{\Omega}_{c,vc}\tilde{\Omega}_{\rm SRS}}{4(\omega-\Delta_1-i\gamma_{vg})(\omega-\Delta_2-i\gamma_{cg})-|\bar{\Omega}_{c,vc}|^2}. \quad (9b)$$

As shown in Eq. (9a), the Raman coherence $\rho_{vg}^{(2)}$ can be suppressed by increasing $\bar{\Omega}_{c,vc}$, i.e., increasing the intensity of the coupling light. Now, we can proceed to the third-order perturbation to calculate SRS signal quantitatively. By introducing a rotating frame $\rho_{ig}^{(3)}=\rho_{ig}^{(3,p)}\exp(-i\omega_p t)+\rho_{ig}^{(3,S)}\exp(i\omega s t)$ and $\rho_{vi}^{(3)}=\rho_{vi}^{(3,p)}\exp(-i\omega_p t)+\rho_{vi}^{(3,S)}\exp(i\omega s t)$, in Fourier space we obtain

$$\tilde{\rho}_{ig}^{(3,p)}(\omega)=\frac{\tilde{\Omega}_{S,iv}*\tilde{\rho}_{vg}^{(2,I)}}{2(\omega_{ig}-\omega_p+\omega-i\gamma_{ig})}, \quad (10a)$$

$$\tilde{\rho}_{ig}^{(3,S)}(\omega)=\frac{\tilde{\Omega}_{p*,iv}*\tilde{\rho}_{vg}^{(2,I)}}{2(\omega_{ig}+\omega_S+\omega-i\gamma_{ig})}, \quad (10b)$$

$$\tilde{\rho}_{vi}^{(3,p)}(\omega)=\frac{-\tilde{\rho}_{vg}^{(2,I)}*\tilde{\Omega}_{S,gi}}{2(\omega_{vi}-\omega_p+\omega-i\gamma_{vi})}, \quad (10c)$$

$$\tilde{\rho}_{vi}^{(3,S)}(\omega)=\frac{-\tilde{\rho}_{vg}^{(2,I)}*\tilde{\Omega}_{p*,gi}}{2(\omega_{vi}+\omega_S+\omega-i\gamma_{vi})}. \quad (10d)$$

Here "$*$" denotes convolution. Since the Rabi frequencies decay rapidly to zero when $|\omega|$ is beyond $1/\tau$, we can omit ω in all the denominators in Eq. (10). Finally, we obtain the third-order nonlinear polarization:

$$\begin{aligned}\tilde{\mathbf{P}}^{(3,p)}(\omega)&=N{\rm tr}\left[\left(\tilde{\rho}_{vi}^{(3,p)}+\tilde{\rho}_{ig}^{(3,p)}\right)\boldsymbol{\mu}\right]\\&=A_S^2A_p\exp\left(-\frac{\omega^2\tau^2}{8\ln 2}\right)\\&\quad *\left[F(\omega)\times\exp\left(-\frac{\omega^2\tau^2}{16\ln 2}\right)\right]\times\mathbf{C}_p, \quad (11a)\end{aligned}$$

$$\begin{aligned}\tilde{\mathbf{P}}^{(3,S)}(\omega)&=N{\rm tr}\left[\left(\tilde{\rho}_{vi}^{(3,S)}+\tilde{\rho}_{ig}^{(3,S)}\right)\boldsymbol{\mu}\right]\\&=A_p^2A_S\exp\left(-\frac{\omega^2\tau^2}{8\ln 2}\right)\\&\quad *\left[F(\omega)\times\exp\left(-\frac{\omega^2\tau^2}{16\ln 2}\right)\right]\times\mathbf{C}_S, \quad (11b)\end{aligned}$$

where N is the number density of the molecule. The response function $F(\omega)$ and the constant vectors $\mathbf{C}_p$, $\mathbf{C}_S$ are expressed in Eqs. (12) and (13), respectively. The decoherence rate has been omitted in Eq. (13) because normally the pump and the Stokes fields are far from resonance to the intermediate states $|i\rangle$, and thus the detuning terms in the denominators are much larger than the decoherence rate.

$$F(\omega)=\frac{2(\omega-\Delta_2-i\gamma_{cg})}{4(\omega-\Delta_1-i\gamma_{vg})(\omega-\Delta_2-i\gamma_{cg})-|\bar{\Omega}_{c,vc}|^2}, \quad (12)$$

$$\begin{aligned}\mathbf{C}_p&=N\frac{\tau^2}{16\hbar^3}\left(\frac{\pi}{\ln 2}\right)^{\frac{3}{2}}\\&\quad\times\sum_i\left[\frac{\boldsymbol{\mu}_{gi}(\mathbf{e}_S\cdot\boldsymbol{\mu}_{iv})}{\omega_{ig}-\omega_p}+\frac{\boldsymbol{\mu}_{iv}(\mathbf{e}_S\cdot\boldsymbol{\mu}_{gi})}{\omega_{iv}+\omega_p}\right]\\&\quad\times\sum_i\left[\frac{(\mathbf{e}_S^*\cdot\boldsymbol{\mu}_{vi})(\mathbf{e}_p\cdot\boldsymbol{\mu}_{ig})}{\omega_{ig}-\omega_p}+\frac{(\mathbf{e}_p\cdot\boldsymbol{\mu}_{vi})(\mathbf{e}_S^*\cdot\boldsymbol{\mu}_{ig})}{\omega_{ig}+\omega_S}\right], \quad (13a)\end{aligned}$$

$$\mathbf{C}_S = N\frac{\tau^2}{16\hbar^3}\left(\frac{\pi}{\ln 2}\right)^{\frac{3}{2}} \times \sum_i\left[\frac{\boldsymbol{\mu}_{gi}(\mathbf{e}_p^*\cdot\boldsymbol{\mu}_{iv})}{\omega_{ig}+\omega_S}+\frac{\boldsymbol{\mu}_{iv}(\mathbf{e}_p^*\cdot\boldsymbol{\mu}_{gi})}{\omega_{iv}-\omega_S}\right] \times \sum_i\left[\frac{(\mathbf{e}_S^*\cdot\boldsymbol{\mu}_{vi})(\mathbf{e}_p\cdot\boldsymbol{\mu}_{ig})}{\omega_{ig}-\omega_p}+\frac{(\mathbf{e}_p\cdot\boldsymbol{\mu}_{vi})(\mathbf{e}_S^*\cdot\boldsymbol{\mu}_{ig})}{\omega_{ig}+\omega_S}\right]. \tag{13b}$$

Now we define the local SRL signal by the change of pump pulse energy per unit volume, which can be calculated as

$$\frac{dE_p}{dV} = \int\frac{dI_p}{dz}dt = -\frac{\omega_p\tau}{4\sqrt{2\pi\ln 2}}\int A_p\exp\left(-\frac{\omega^2\tau^2}{8\ln 2}\right) \times \mathrm{Im}[\tilde{\mathbf{P}}^{(3,p)}(\omega)\cdot\mathbf{e}_p^*]d\omega = -\frac{\sqrt{2}}{4}\omega_p\mathbf{C}_p\cdot\mathbf{e}_p^*A_p^2A_S^2\int\mathrm{Im}[F(\omega)] \times\exp\left(-\frac{\omega^2\tau^2}{8\ln 2}\right)d\omega, \tag{14a}$$

where I_p is the intensity of the pump beam; z is the propagation direction of the pump and Stokes beams. Normally, $\boldsymbol{\mu}_{iv}$ is parallel to $\boldsymbol{\mu}_{ig}$ (cf. Appendix A of Ref. [16]), and so $\mathbf{C}_p\cdot\mathbf{e}_p^*$ is a real and positive constant. Thus in the last step, we move $\mathbf{C}_p\cdot\mathbf{e}_p^*$ outside the integral. Equation (14a) apparently describes a loss of the pump field. Similarly, the local SRG signal can be defined by the change of Stokes pulse energy per unit volume:

$$\frac{dE_S}{dV} = \frac{\sqrt{2}}{4}\omega_S\mathbf{C}_S\cdot\mathbf{e}_SA_p^2A_S^2\int\mathrm{Im}[F(\omega)]\exp\left(-\frac{\omega^2\tau^2}{8\ln 2}\right)d\omega, \tag{14b}$$

Here $\mathbf{C}_S\cdot\mathbf{e}_S$ is real and positive, and Eq. (14b) describes a gain of the Stokes field. Equation (14) provides a general description of the SRS signal with a coupling level and a coupling field in our scheme, based on which we can derive the behavior of SRS signal under different conditions. Figures 2(a)–2(c) show the relative SRS signal vs $|\bar{\Omega}_{c,cv}|$ and τ for three different cases: (1) $\gamma_{cg}=0.1\gamma$, $\gamma_{vg}=10\gamma$; (2) $\gamma_{cg}=\gamma_{vg}=\gamma$; (3) $\gamma_{cg}=10\gamma, \gamma_{vg}=0.1\gamma$. Conditions (1)–(3) correspond to the cases where the coherence between states $|c\rangle$ and $|g\rangle$ lasts longer than, equal to, or shorter than that between states $|v\rangle$ and $|g\rangle$, respectively. We set the detuning $\Delta_1=\Delta_2=0$. The relative SRS signal is evaluated by the integral in Eq. (14), and for each τ it is normalized to the value when there is no coupling light. Therefore, the relative SRS signal shows the relative change of SRS when the coupling light is applied. Clearly Fig. 2 shows that the SRS signal can be suppressed when $|\bar{\Omega}_{c,cv}|$ and τ are large enough.

In order to understand the effects of $\bar{\Omega}_{c,cv}$, it is helpful to look into the properties of $\mathrm{Im}[F(\omega)]$ in Eq. (14). As shown in Figs. 2(d)–2(f), for a higher Rabi frequency of the coupling field, $\mathrm{Im}[F(\omega)]$ is smaller around $\omega=0$. According to Eq. (12), $\mathrm{Im}[F(0)]$ decreases by half when $|\bar{\Omega}_{c,cv}|$ is equal to $2(\gamma_{cg}\gamma_{vg})^{1/2}$. Hence, this value can be regarded as a critical value at which the SRS signal is suppressed by half for CW

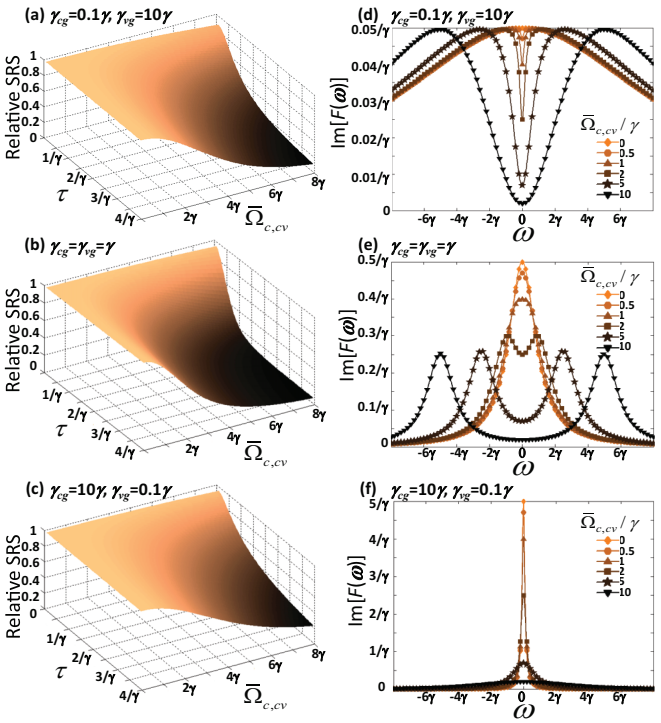

FIG. 2. (Color online) (a–c) the relative SRS signal vs $|\bar{\Omega}_{c,cv}|$ and τ; (d–f) the profiles of $\mathrm{Im}[F(\omega)]$ for different Rabi frequency of the coupling laser $|\bar{\Omega}_{c,cv}|$. (a, d): $\gamma_{cg}=0.1\gamma$, $\gamma_{vg}=10\gamma$; (b, e): $\gamma_{cg}=\gamma_{vg}=\gamma$; (c, f): $\gamma_{cg}=10\gamma$, $\gamma_{vg}=0.1\gamma$.

excitations:

$$|\bar{\Omega}_{c,cv}|_{\mathrm{critical}} = 2\sqrt{\gamma_{vg}\gamma_{cg}}. \tag{15}$$

To understand the effects of τ, we need to look into the shape of the $\mathrm{Im}[F(\omega)]$ profile which is determined by ω_0 in Eq. (16). If it is real, two peaks will appear at $\pm\omega_0$ as seen in Figs. 2(d) and 2(e). When the coupling field is weak or γ_{cg} is relatively large, ω_0 becomes imaginary, and the profile will be broadened without two separated peaks, as in Fig. 2(f).

$$\omega_0 = \sqrt{\frac{|\bar{\Omega}_{c,cv}|^2}{4\gamma_{vg}}\left[(\gamma_{cg}+\gamma_{vg})\sqrt{1+\frac{\gamma_{cg}\gamma_{vg}}{|\bar{\Omega}_{c,cv}|^2}}-\gamma_{cg}\right]-\gamma_{cg}^2}. \tag{16}$$

According to Eq. (14), reducing the overlapping between $\mathrm{Im}[F(\omega)]$ and the Gaussian excitation spectrum $\exp(-\omega^2\tau^2/8\ln 2)$ is the key to suppressing SRS. A small τ always reduces the suppression efficiency because a broad excitation spectrum can have significant overlap with a broadened $\mathrm{Im}[F(\omega)]$ profile or its two peaks at $\pm\omega_0$. A larger τ is always beneficial for the suppression of SRS signal.

Thus we can define a critical value τ_{critical} which makes the half width at half maximum (HWHM) of the excitation spectrum equal to ω_0 or the HWHM of $\mathrm{Im}[F(\omega)]$ when there is no coupling field, whichever is larger:

$$\tau_{\mathrm{critical}} = 2\sqrt{2}\ln 2\left(\max\left[\frac{1}{\gamma_{vg}},\frac{1}{\omega_0}\right]\right) \approx 1.96\left(\max\left[\frac{1}{\gamma_{vg}},\frac{1}{\omega_0}\right]\right). \tag{17}$$

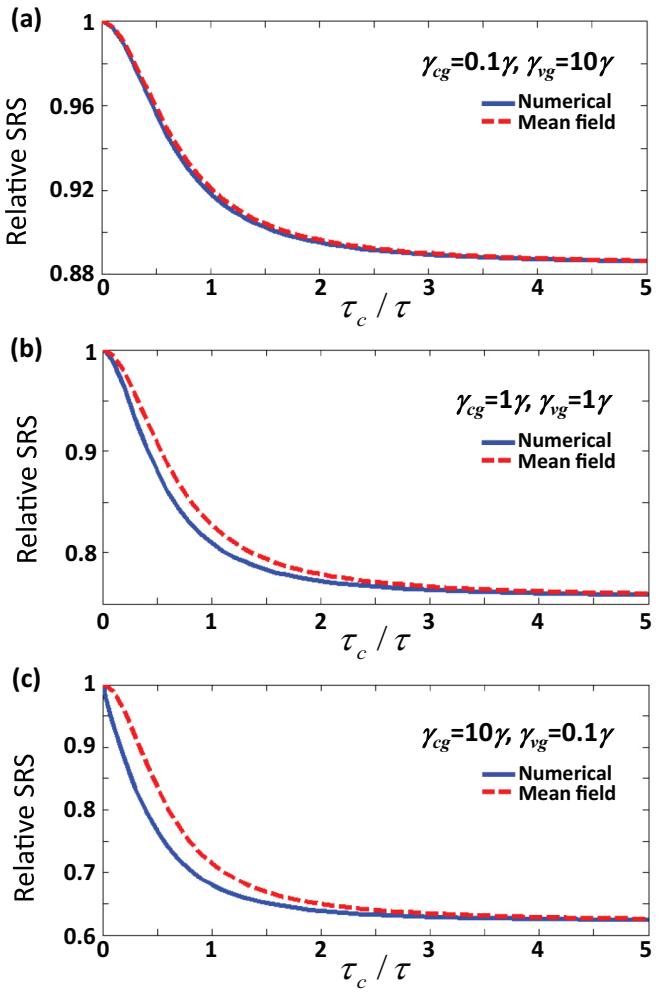

FIG. 3. (Color online) Relative SRS signal as a function of τ_c/τ, for three different cases: (a) $\gamma_{cg} = 0.1\gamma$, $\gamma_{vg} = 10\gamma$; (b) $\gamma_{cg} = \gamma_{vg} = \gamma$; and (c) $\gamma_{cg} = 10\gamma$, $\gamma_{vg} = 0.1\gamma$. Both the numerical results and the mean-field results are plotted.

In practice, it is desirable to set τ equal to or larger than τ_{critical}.

As discussed earlier, the pulse duration of the coupling laser τ_c is assumed to be much larger than the duration of pump and Stokes lasers τ to satisfy adiabatic approximation. However, larger τ_c also leads to higher pulse energy, which may cause photodamage in experiment. Thus we need to set τ_c as small as possible while keeping the suppression of the SRS signal efficient. For this purpose, the relative SRS signal vs τ_c/τ is calculated. Equation (6) can be analytically solved with our mean-field approach, but this approach is not accurate when τ_c/τ is small. Therefore we also solved Eq. (6) numerically. Both numerical and mean-field results are plotted in Fig. 3. $|\bar{\Omega}_{c,cv}|$ and τ are set at the critical value. The results show that when τ_c is twice of τ, the suppression of SRS becomes roughly saturated.

As a brief summary of this section, we have theoretically demonstrated that the SRS can be effectively suppressed by applying a coupling field between the vibrational state $|v\rangle$ and a coupling state $|c\rangle$. The strategy of choosing parameters is as follows: (1) $|\bar{\Omega}_{c,cv}|$ and τ should be no less than the critical value. (2) τ_c can be set at 2τ. In this case, $|\bar{\Omega}_{c,cv}| = 0.9428 A_c \mathbf{e}_c \cdot \boldsymbol{\mu}_{cv}/\hbar$. (3) The pump and Stokes lasers should be weak enough to be regarded as perturbations. In other words, the SRS process should be far from saturation; i.e., the peak intensities of pump and Stokes lasers should be much smaller than $10^{12}\,\text{W/cm}^2$ [16]. (4) Normally, RWA will start to fail if the laser intensity $> 10^{14}\,\text{W/cm}^2$ [25], and so the peak intensities of all three pulses should be much smaller than this value.

III. CASE STUDY FOR DPPC

In the following, we will present a numerical study on the resolution enhancement when our scheme is implemented in a STED-like super-resolution SRS microscope. A target molecule with a coupling state must be identified, and the parameters of excitation lasers must be chosen accordingly. In this study, we will use dipalmitoylphosphatidylcholine (DPPC) as the target molecule. DPPC is a common lipid, and it has a strong CH_2 symmetric stretching Raman band which is widely used for imaging lipids in SRS and CARS microscopy. We performed Fourier transform infrared (FTIR) measurements to obtain the parameters of this Raman band, the details of which are described in the Appendix: the Raman shift is $2856\,\text{cm}^{-1}$, corresponding to $\omega_{vg} = 538.34\,\text{THz}$; the ransition dipole moment $\mu_{vg} = 2.16 \times 10^{-3}\,e\,\text{nm}$; the decoherence rate $\gamma_{vg} = 0.96\,\text{ps}^{-1}$.

Now a coupling state has to be identified. First of all, dipole transition must be allowed between the vibrational state $|v\rangle$ and the coupling state $|c\rangle$. Secondly, ω_{cv} must avoid any absorption peaks from the ground state. Hence the first overtone vibrational state and the lowest dipole-transition-allowed electronic state can be considered as two candidates. We will discuss them separately.

The first overtone vibrational state of C-H symmetric stretching in CH_2 is at $5591\,\text{cm}^{-1}$, which means that $\omega_{cv} = 515.54\,\text{THz}$ and $\lambda_c = 3566\,\text{nm}$. As described in the Appendix, we have $\boldsymbol{\mu}_{cv} = 3.08 \times 10^{-3} e\,\text{nm}$ and $\gamma_{cg} = 2.21\,\text{ps}^{-1}$. According to Eq. (15), the critical Rabi frequency of the coupling field is $|\bar{\Omega}_{c,cv}|_{\text{critical}} = 2.92\,\text{ps}^{-1}$. Assuming that the polarization of the coupling laser is parallel to the dipole momentum μ_{cv}, the critical peak intensity of the coupling laser is calculated to be $I_{c\_\text{critical}} = \varepsilon_0 c n A_c^2/2 = 8.48 \times 10^{10}\,\text{W/cm}^2$, where ε_0 is the vacuum permittivity; c is the speed of light in vacuum; and $n = 1.46$ is the typical refractive index for lipids [28]. When $I_c = I_{c\_\text{critical}}$, we get $\tau_{\text{critical}} = 2.04\,\text{ps}$ by Eq. (17). This is the suggested minimal FWHM duration for the pump and Stokes lasers, and based on Fig. 3 the duration of the coupling laser needs to be twice that value.

On the other hand, the lowest dipole-transition-allowed electronic state of DPPC produces an absorption peak at 192 nm in UV-vis absorption measurements. As described in the Appendix, $\mu_{cv} = 3.58 \times 10^{-2} e\,\text{nm}$, $\gamma_{cg} = 255.66\,\text{ps}^{-1}$, and $\lambda_c = 203\,\text{nm}$. Following the same procedure described above, we find the critical peak intensity of the coupling field $I_{c\_\text{critical}} = 1.29 \times 10^{11}\,\text{W/cm}^2$. When $I_c = I_{c\_\text{critical}}$, $\tau_{\text{critical}} = 2.04\,\text{ps}$ still.

All the calculations above are based on parameters measured at room temperature. In condensed matter, the decoherence between states is mainly caused by molecular collision,

which will be smaller when the temperature is lower. Therefore at lower temperature, lower $I_{c\_critical}$ is expected.

In both cases at room temperature, we need 4-ps coupling laser with a peak intensity of $\sim 10^{11}$ W/cm^2. The wavelength of the coupling laser is either UV or mid-IR. For microscopy applications, the construction of such a laser source and its coupling into a microscope may pose technical challenges. Furthermore, in a complex sample, the absorption from other molecules at these wavelengths may also become a practical limitation. In the super-resolution SRS microscopy simulation below, we assume that all the excitation lasers are already focused into the sample and the resolution arising from the SRS signal of the target molecules is calculated.

IV. APPLICATION IN SUPER-RESOLUTION SRS MICROSCOPY

To achieve super-resolution in SRS microscopy, we can use a STED-like setup in which a donut-shaped coupling laser is focused into the sample together with the normal pump and Stokes lasers. The coupling laser will suppress the SRS signal at the rim part of the focal spot, reducing the size of the excitation volume and leading to super-resolution.

Experimentally the donut-shaped coupling beam can be produced by a phase plate with a helical phase ramp $\exp(i\phi)$ combined with a quarter-wave plate. This method is widely used in STED microscopy [29–31]. With the quarter-wave plate the coupling beam is circularly polarized. We assume all three beams are focused onto the sample by an objective with

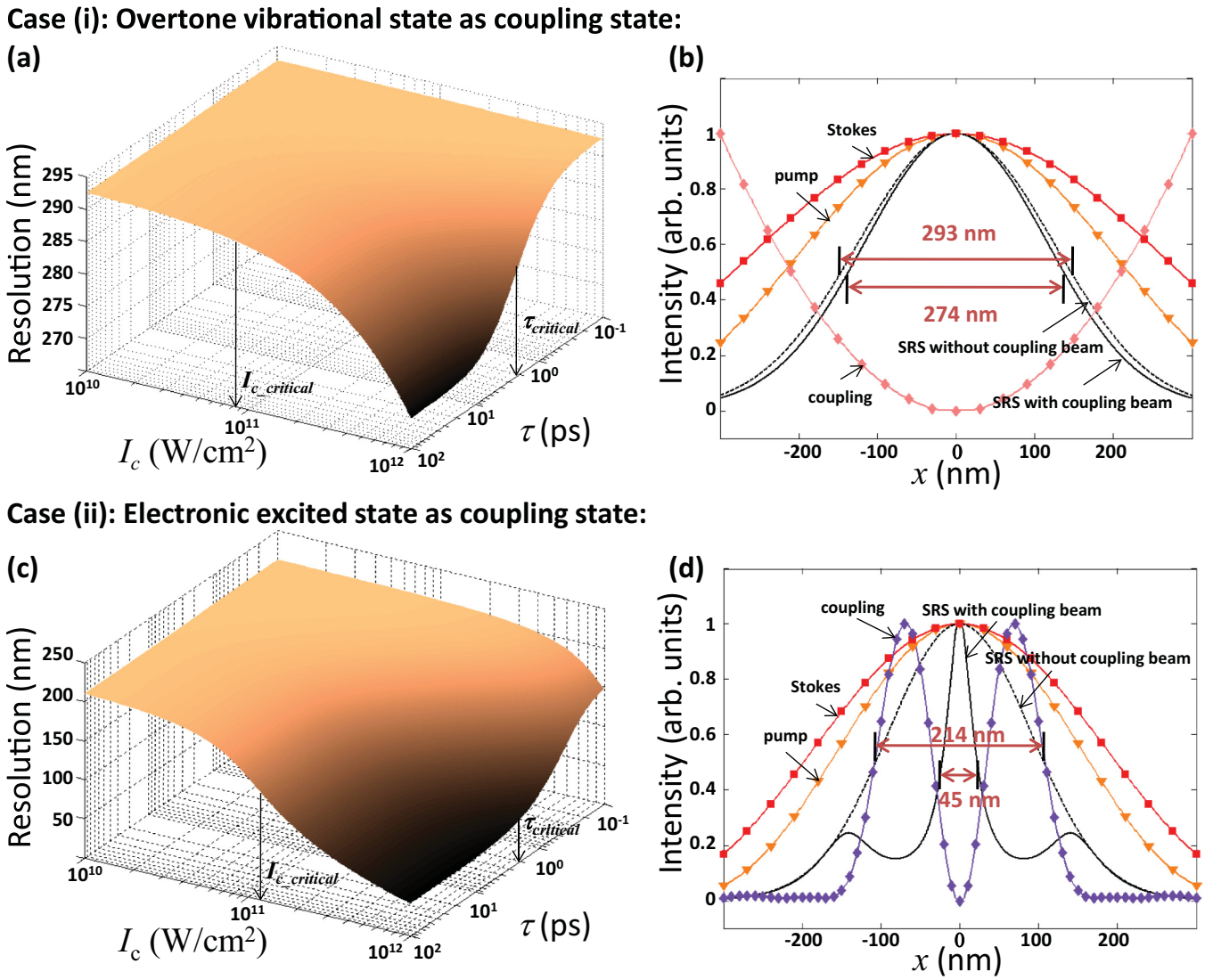

FIG. 4. (Color online) (a, c) The resolution as a function of the peak intensity of the coupling beam I_c and the pulse duration of the pump and Stokes lasers $\tau(\tau_p = \tau_S = \tau)$ for case (i) and (ii), respectively. The pulse duration of the coupling laser τ_c is set at 2τ. (b, d), Cross sections of the normalized intensity profiles along the x axis on the focal plane when $\tau_S = \tau_p = 5$ ps, $\tau_c = 10$ ps, and $I_c = 10^{12}$ W/cm^2: pump beam (triangles), Stokes beam (squares), coupling beam (diamonds), SRS intensity without the coupling beam (dashed curve), and SRS intensity with the coupling beam (solid curve). (a, b) are for case (i): $\lambda_p = 800$ nm, $\lambda_S = 1037$ nm, $\lambda_c = 3566$ nm. (c, d) are for case (ii): $\lambda_p = 600$ nm, $\lambda_S = 724$ nm, $\lambda_c = 203$ nm.

numerical aperture (NA) = 1.2. The polarization of pump and Stokes lasers is set to be along the x axis before the objective. The method to calculate the electric field distribution of the three beams in the focal region was described in our previous work [16]. Then the SRS signal intensity at the focal plane is calculated. The sample is assumed to be isotropic, and so the SRS intensity is an average value for dipole moments orientated in the x, y, and z directions. At last we acquire the lateral resolution defined as the FWHM of the SRS intensity profile along the x axis on the focal plane.

We calculated the resolution for the two cases of coupling state: (i) the first overtone vibrational state and (ii) the lowest dipole-transition-allowed electronic state. In case (i), we set $\lambda_p = 800\,\text{nm}$ and $\lambda_S = 1037\,\text{nm}$, since they are typical wavelengths to image Raman shift $2856\,\text{cm}^{-1}$ in SRS microscopy. However, in case (ii), we found that these wavelengths are no longer suitable because the donut-shaped coupling beam at $\lambda_c = 203\,\text{nm}$ becomes too thin and if we still set $\lambda_p = 800\,\text{nm}$ the SRS signal outside the donut beam will still be strong. Therefore, the pump and Stokes wavelengths have to be reduced in this case and we set $\lambda_p = 600\,\text{nm}$ and $\lambda_S = 724\,\text{nm}$ instead.

Figures 4(a) and 4(c) plots the resolution as a function of the peak intensity of the coupling beam I_c and the pulse duration of pump and Stokes lasers $\tau(\tau_p = \tau_S = \tau)$ for case (i) and case (ii), respectively. τ_c is set at 2τ according to the conclusion in Sec. II. In both cases, the resolution is gradually improved when I_c is larger than $I_{c\text{-critical}}$ and τ is larger than τ_{critical}. Figures 4(b) and 4(d) plot the intensity profiles along the x axis on the focal plane for the pump, Stokes, and coupling lasers, as well as the SRS signal with and without the coupling laser for case (i) and (ii), respectively. Here we set $\tau_S = \tau_p = 5\,\text{ps}$ as it is a typical pulse duration for ps lasers. For the coupling laser, $\tau_c = 10\,\text{ps}$ and $I_c = 10^{12}\,\text{W/cm}^2$. We can see that in case (i), the introduction of the coupling laser only provides a minor enhancement of resolution from 293 to 274 nm, while in case (ii), a significant resolution enhancement from 214 nm down to 45 nm is achieved. We should also note, however, that there is still some residue SRS signal outside the donut beam, which appears as side lobes in Fig. 2(d). The side lobe intensity is about 20% of the central peak. A smaller λ_p helps to suppress the side lobes. If we set $\lambda_p < 2.23\lambda_c$ or less than 453 nm here, the SRS intensity at the side lobe would be less than $\frac{1}{10}$ of the central peak.

This difference in resolution enhancement can be easily understood if we compare the profiles of the coupling laser in Figs. 4(b) and 4(d). The peaks of the donut-shaped beam in Fig. 4(d) are apparently much sharper, because λ_c in case (ii) is much shorter. Hence the resolution enhancement in case (ii) is much higher at the same peak intensity. In other words, to achieve the same resolution enhancement in case (i) we need a coupling beam with much higher intensity. But on the other hand, case (ii) has the disadvantage that at least two of the three excitation wavelengths are in the UV or visible region, and high-intensity laser pulses at these wavelengths may easily cause photodamage to samples. Case (i) may be safer because two of the wavelengths are in the NIR window. The third one is mid-IR, which may cause significant water absorption but is relatively safe otherwise. In the end, the choice of the wavelengths relies on the absorption properties of the actual sample and the transmission properties of the imaging setup for a real application.

V. CONCLUSION

In summary, we have presented a theoretical study on the suppression of SRS by an EIT-like scheme and its application in super-resolution imaging. Besides the pump and Stokes lasers, we propose that introducing a third laser which couples the vibrational state to a coupling state can effectively suppress the SRS signal, if the following four conditions are satisfied: (1) The peak intensity of the pump and Stokes pulse should be small enough to be considered as perturbation; (2) the peak intensity of the coupling laser and the pulse duration of the pump and Stokes lasers should be larger than a critical value; (3) the pulse duration of the coupling laser should be at least twice that of pump and Stokes pulses; (4) the peak intensities of all three pulses should be small enough to satisfy RWA.

Using DPPC molecule and SRS from its CH_2 symmetric stretching vibration as a real example, we found that it is theoretically possible to use its first overtone vibrational state or the lowest electronic state as the coupling state. In both cases the critical coupling laser intensity is about $10^{11}\,\text{W/cm}^2$ and the critical pump and Stokes pulse duration is about 2 ps.

In principle this EIT-like scheme can be used to break the diffraction limit in SRS microscopy by introducing a donut-shaped coupling beam. Our calculation shows that the lateral resolution can be significantly enhanced by choosing the lowest electronic excited state as the coupling state and a coupling laser intensity of about $10^{12}\,\text{W/cm}^2$.

Among different super-resolution CARS and SRS schemes, our scheme has the unique feature that most of the target molecules are kept at the ground state, thus avoiding their photodamage. But on the other hand there are also technical challenges such as finding a proper coupling laser and achieving good microscope transmission. We believe that it is possible to experimentally realize this scheme in the future for specific types of samples, where enhanced resolution is desired for more information.

ACKNOWLEDGMENTS

This work was supported by a NUS FoS Tier 1 grant (Grant No. R144000337112).

APPENDIX

In this Appendix, the methods of how to obtain the parameters used in Sec. III are briefly introduced, including ω_{ij}, γ_{ij}, and μ_{ij}.

We measured the IR spectrum of DPPC powder by a Thermo Nicolet 380 FTIR spectrometer, equipped with a MCT-A detector and a Slide-on ATR attachment (Ge crystal tip). We also measured the UV-vis spectrum of DPPC dissolved in ethanol-water (9:1, v/v) by a Cary 50 UV-vis spectrophotometer. All the absorption peak positions can be directly read from the spectra, from which we know ω_{ij}. All the decoherent rates γ_{ij} can be calculated from the FWHM of the

peaks. From the spectrum, measuring geometry, and sample concentration, we can also get the absorption cross section σ_{ij} per C-H bond in the CH_2 group. Then, we can calculate μ_{ij} from σ_{ij} by [32]

$$\mu_{ij} = \sqrt{2\varepsilon_0 \hbar \gamma_{ij} \sigma_{ij} \lambda_{ij}}, \tag{A1}$$

where λ_{ij} is the transition wavelength.

From FTIR spectra, we know that σ_{vg} is $1.90 \times 10^{-19}\,\mathrm{cm}^2$. Thus we know $\mu_{vg} = 2.16 \times 10^{-3} e\,\mathrm{nm}$.

If the first overtone vibrational state is used as the coupling state, we cannot measure σ_{cv} directly. An indirect method is needed to obtain μ_{cv}. Normally, the Morse potential is a good description of the vibration of chemical bond [33]. Base on the theory of the Morse potential, if we know μ_{vg}, μ_{cv} can be calculated by

$$\frac{\mu_{cv}}{\mu_{vg}} = \frac{2N-1}{2N-3}\sqrt{2\frac{N-2}{N}\frac{\Gamma(2N-1)\Gamma(2N+1)}{[\Gamma(2N)]^2}}, \tag{A2}$$

where $N = 1.5 k_{vg}/(k_{vg} - k_{cv}) = 24.10$; k is the wave number. Thus we obtain $\mu_{cv} = 1.4291 \mu_{vg} = 3.08 \times 10^{-3} e\,\mathrm{nm}$.

If the dipole-transition-allowed electronic state is used as the coupling state, from the UV-vis spectrum we have $\sigma_{gc} = 3.59 \times 10^{-18}\,\mathrm{cm}^2$. Thus we know $\mu_{gc} = 3.58 \times 10^{-2} e\,\mathrm{nm}$ by Eq. (A1). Under the Born-Oppenheimer approximation, $|g\rangle$ and $|v\rangle$ share the same electronic structure. Since μ_{gc} and μ_{cv} are dominated by the electronic part rather than the nuclear part, we have approximately $\mu_{cv} = \mu_{gc} = 3.58 \times 10^{-2}\,e\,\mathrm{nm}$.

[1] J.-X. Cheng and X. S. Xie, J. Phys. Chem. B **108**, 827 (2003).
[2] J.-X. Cheng, A. Volkmer, and X. S. Xie, J. Opt. Soc. Am. B **19**, 1363 (2002).
[3] C. W. Freudiger, W. Min, B. G. Saar, S. Lu, G. R. Holtom, C. He, J. C. Tsai, J. X. Kang, and X. S. Xie, Science **322**, 1857 (2008).
[4] P. Nandakumar, A. Kovalev, and A. Volkmer, New J. Phys. **11**, 033026 (2009).
[5] S. W. Hell and J. Wichmann, Opt. Lett. **19**, 780 (1994).
[6] M. J. Rust, M. Bates, and X. Zhuang, Nat. Methods **3**, 793 (2006).
[7] P. Kner, B. B. Chhun, E. R. Griffis, L. Winoto, and M. G. L. Gustafsson, Nat. Methods **6**, 339 (2009).
[8] W. P. Beeker, P. Groß, C. J. Lee, C. Cleff, H. L. Offerhaus, C. Fallnich, J. L. Herek, and K.-J. Boller, Opt. Express **17**, 22632 (2009).
[9] W. P. Beeker, C. J. Lee, K.-J. Boller, P. Groß, C. Cleff, C. Fallnich, H. L. Offerhaus, and J. L. Herek, Phys. Rev. A **81**, 012507 (2010).
[10] K. M. Hajek, B. Littleton, D. Turk, T. J. McIntyre, and H. Rubinsztein-Dunlop, Opt. Express **18**, 19263 (2010).
[11] W. P. Beeker, C. J. Lee, K. J. Boller, P. Groß, C. Cleff, C. Fallnich, H. L. Offerhaus, and J. L. Herek, J. Raman Spectrosc. **42**, 1854 (2011).
[12] C. Cleff, P. Groß, C. Fallnich, H. L. Offerhaus, J. L. Herek, K. Kruse, W. P. Beeker, C. J. Lee, and K.-J. Boller, Phys. Rev. A **86**, 023825 (2012).
[13] C. Cleff, P. Groß, C. Fallnich, H. L. Offerhaus, J. L. Herek, K. Kruse, W. P. Beeker, C. J. Lee, and K.-J. Boller, Phys. Rev. A **87**, 033830 (2013).
[14] W. Liu and H. Niu, Phys. Rev. A **83**, 023830 (2011).
[15] V. Raghunathan and E. O. Potma, J. Opt. Soc. Am. A **27**, 2365 (2010).
[16] L. Gong and H. Wang, Phys. Rev. A **90**, 013818 (2014).
[17] S. E. Harris, J. E. Field, and A. Imamoğlu, Phys. Rev. Lett. **64**, 1107 (1990).
[18] S. E. Harris, Phys. Today **50**, 36 (1997).
[19] M. Fleischhauer, A. Imamoglu, and J. P. Marangos, Rev. Mod. Phys. **77**, 633 (2005).
[20] R. W. Boyd, *Nonlinear Optics*, 3rd ed. (Academic Press, Elsevier, Amsterdam, 2010).
[21] A. Volkmer, L. D. Book, and X. S. Xie, Appl. Phys. Lett. **80**, 1505 (2002).
[22] J. H. Eberly, M. L. Pons, and H. R. Haq, Phys. Rev. Lett. **72**, 56 (1994).
[23] S. E. Harris, Phys. Rev. Lett. **72**, 52 (1994).
[24] D. D. Yavuz, Phys. Rev. A **75**, 031801 (2007).
[25] L. E. E. de Araujo, Phys. Rev. A **69**, 013408 (2004).
[26] V. V. Kozlov and J. H. Eberly, Opt. Commun. **179**, 85 (2000).
[27] L. E. E. de Araujo, Phys. Rev. A **73**, 053821 (2006).
[28] W. Yassine, A. Milochau, S. Buchoux, J. Lang, B. Desbat, and R. Oda, Biochim. Biophys. Acta, Biomembr. **1798**, 928 (2010).
[29] S. Bretschneider, C. Eggeling, and S. W. Hell, Phys. Rev. Lett. **98**, 218103 (2007).
[30] B. Harke, J. Keller, C. K. Ullal, V. Westphal, A. Schönle, and S. W. Hell, Opt. Express **16**, 4154 (2008).
[31] G. Vicidomini, A. Schönle, H. Ta, K. Y. Han, G. Moneron, C. Eggeling, and S. W. Hell, PloS One **8**, e54421 (2013).
[32] P. Meystre and M. Sargent, *Elements of Quantum Optics*, 3rd ed. (Springer, Berlin, 1998).
[33] E. F. d. Lima and J. E. M. Hornos, J. Phys. B: At., Mol. Opt. Phys. **38**, 815 (2005).